Final Technical Report

Federal Agency	**Department** of Energy – National Energy Technology Laboratory (NETL)
FOA Name and Number	Fiscal Year (FY) 2019 Vehicle Technologies Program Wide Funding Opportunity Announcement (FOA) No. DE-FOA-0002014
Nature of the Report	Final Technical Report
Award Number	**DE-EE0008863**
Award Type	Cooperative Agreement
Prime Recipient Type	Private Company
Prime Recipient	General Motors LLC
Principal Investigator & Prime Recipient Technical Contact Information	**Dr. Xingcheng Xiao** Technical Fellow GM Global Research and Development 30500 Mound Road Warren, Michigan 48092-2031 Tel: (248) 912-8132 Email: xingcheng.xiao @gm.com
Contract Manager & Prime Recipient Business Contact Information	Aida Rodrigues Manager – Government Contracts General Motors LLC 850 North Glenwood Avenue Pontiac, MI 48340-2920 Tel: (585) 303-6601 Email: aida.rodrigues@gm.com
Project Team	Brown University and University of Kentucky
Project Title	**Fundamental Understanding of Dynamic Interfacial Phenomena in Solid State Batteries**
Prime Recipient's DUNS No.	784804056
Date of the Report	August 27, 2023
Period of Performance	10/01/2019 – 05/31/2023

1. PROJECT BACKGROUND

Solid-state batteries (SSBs) are considered the next generation battery technology for resolving the intrinsic limitations of current lithium-ion batteries, such as poor abuse tolerance, insufficient energy density, and short cycle life. However, the main hurdle for SSB in electric vehicle (EV) applications is the complexity caused by material interfaces, such as Li metal/solid electrolyte (SE) and SE/cathode interfaces, leading to increased impedance and shortened cycle life. **Figure 1** shows the main degradation mechanism associated with interfaces in SSB, such as stresses at the interface caused by volume changes, contact area loss due to the mechanical properties mismatch, impendence increase of ion diffusion by interlayers or the space charge layer, and side reactions by element inter-diffusion. Although interfaces in SSBs are one of the key factors, a clear understanding of their properties and functions is still unavailable, partly due to the difficulty in characterizing buried solid-solid interfaces and interphases formed during battery cycling.

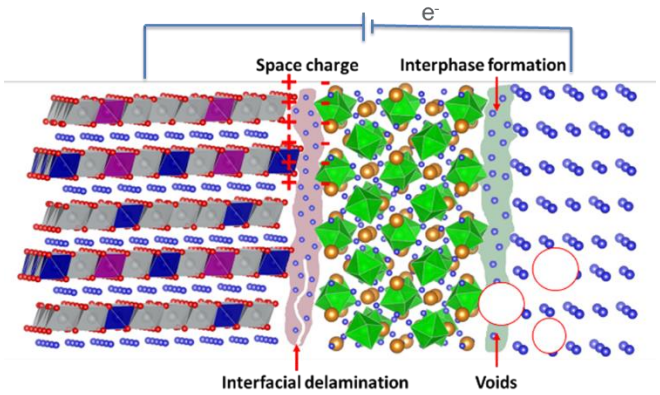

Figure 1. the main degradation mechanism associated with interface in all solid-state batteries.

An effective strategy for interface engineering will not only prevent detrimental interphase formation, but also accommodate volume change from both Li and cathodes while maintaining intimate physical contact and facilitate charge transfer / suppress space charge. To accomplish this, several critical barriers need to be addressed:

- The mechanical compatibilities at interfaces of Li/SEs and SE/cathode materials are not well understood. Incompatibilities can lead to void formation and interfacial delamination during Li plating/stripping processes since both the Li anode and cathode have significant volume expansion and contraction. The characterization of interfacial mechanical properties, such as elastic modulus, hardness, fracture toughness, and stress, is a "grand challenge."
- The evolution of the structure and composition of the interface/interphase with cycle number is closely coupled to non-uniform current distribution that depends on Li diffusion through SEs, Li plating/stripping kinetics, and Li intercalation kinetics at the cathode. The dynamic relationships between these processes and the interface mechanical property evolution have not been studied in detail.
- Interfaces were embedded in the cell, which makes it extremely difficult to apply traditional characterization techniques investigate the mechanical/transport properties around the interfaces locally. A well-controlled platform combining with in situ characterization is

needed to conduct fundamental investigations of the coupled dynamic mechanical/chemical properties of the SEs with the anode and cathode in an electrochemical environment.

2. OBJECTIVES

The project objective is to develop a comprehensive set of in situ diagnostic techniques combined with atomic/continuum modeling schemes to investigate and understand the coupled mechanical/chemical degradation associated with dynamic interfacial phenomena in SSBs. Specifically, in situ observations and characterizations of lithium plating-stripping processes, lithium dendrite formation, interphase formation, and the induced interfacial stresses, as well as the mechanical and electrochemical properties of interfaces and interphases, are paramount. The study will provide useful guidelines for optimizing cell structure design and engineering interfaces and interphases to enable SSBs. In addition, it will establish a critical guideline to design safe and durable SSBs with energy density > 500 wh/kg for EV applications. To achieve that, the following research directions were proposed and executed during the 3 budget periods, including:

- Develop a comprehensive diagnostic mythology integrated with mechanical-chemo characterization capability and multiscale modeling, to understand solid state battery failure mechanism.
- Clarify critical mechanical/chemical/transport proprieties responsible for the interfacial degradation in solid state batteries.
- Establish interfacial stabilization strategies and design space based on multiscale modeling.
- Develop multifactional layers which can improve the mechanical and chemical stability of interfaces and facilitate charge transfer in solid state batteries.

3. APPROCHES

The multiscale *in situ* diagnostic tools, including AFM, nanoindentation, dilatometer, stress sensors, and pressure cells, will be used to investigate the mechanical behavior and the microstructure evolution at interface/interphase during the Li plating and stripping. The information, along with Li ion transport properties and microstructure evolution obtained using the advanced spectroscopic ellipsometry, and *in situ* TEM, will be correlated with electrochemical performance towards high cycle efficiency and dendrite free SSBs. The goal of this understanding is to develop strategies for surface and interface engineering, apply to the commercially available SEs (including powder, pellets, and foils) and assemble to SSB for further validation and optimization, and eventually extend the cycle life of SSBs for EV application.

Figure 2 outlines our strategy to understand the coupled mechanical/chemical degradation of interface/interphase in SSBs, especially the time-dependent dynamic phenomena. To overcome the technical challenges listed in the Background, we have

i. **Developed well-controlled electron/SE interface and Li/SEs/cathode SSB model systems** enabled by GM's unique integrated PVD-glovebox system, which enable us to investigate critical interfacial dynamic behavior in an electrochemical environment.
ii. **Developed a comprehensive set of *in situ* mechanical diagnostic techniques** (including AFM, nanoindentation, dilatometer, and stress sensors, and pressure cells) to capture the critical mechanical properties and coupled chemical-mechanical failure mechanisms from the interface to the cell level.

iii. **Revealed the chemistry and dynamics of interface/interphase** via advanced postmortem analysis tools, such as ToF-SIMS, HRTEM, and the first XPS-Raman system USA.
iv. **Established a multiscale modelling framework** to integrate the chemical and mechanical stability of the interface and to correlate the mechanistic understanding from various diagnostic methods.
v. **Developed an interlayer design strategy to stabilize both interfaces** into SSBs based on the in-situ understanding as the end of a full loop.

Further validation went through the same loop, so we were able to optimize the interface engineering strategy. Our goal is to deliver a tool package integrated with mechanical-chemo characterization capability and multiscale modeling, which enable us to design the SSBs to achieve high cycle efficiency (dendrite-free) Li metal-based rechargeable SSBs with >350 Wh/kg energy density for EV applications.

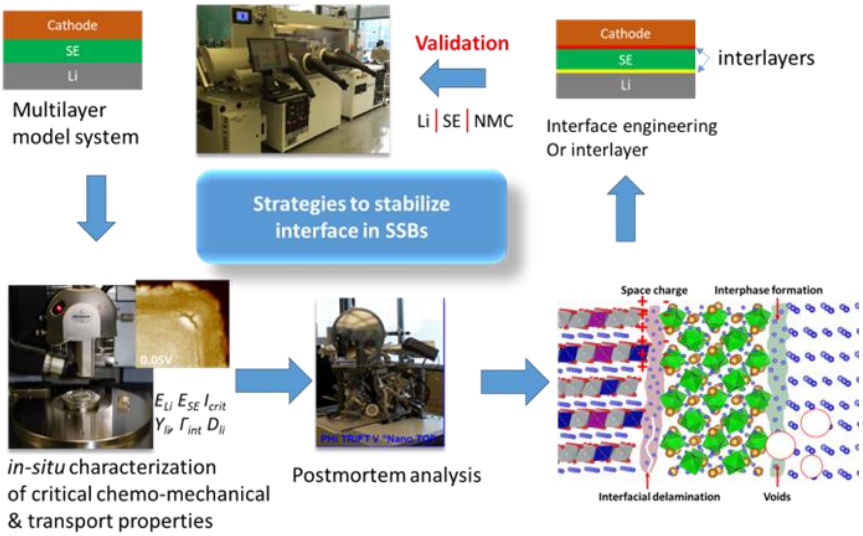

Figure Error! Use the Home tab to apply 0 to the text that you want to appear here.**2. The strategics approach to fundamental understand the interfacial phenomena in solid state batteries and develop the mitigation strategies.**

4. ACCOMPLISHMENTS

4.1 Developed a comprehensive tool set to develop SSB model system and in-situ characterization capability.

A key challenge associated with identifying the governing failure modes is the lack of a well-controlled system that can enable a quantitative assessment of the coupled mechanical and chemical behavior associated with interface phenomena. Investigating interface in a sandwich SSB in an electrochemical environment is particularly difficult because the interface/interphase is extremely thin and concealed by the electrodes and SEs, Li is very soft, and most of SEs and cathodes are air/moisture sensitive. These factors make it difficult to use conventional techniques to characterize and decouple the mechanical/chemical properties of interface/interphase.

During the past three years, GM team has developed the PVD systems integrated with glovebox (as shown in **Figure 3**) which provide us a unique capability to deposit Li/SE and

SE/cathode interphases with controlled kinetics and deposit the entire Li/SE/Cathode SSB model system in well controlled environment, as these materials are sensitive to oxygen, moisture, and CO_2. The subsequent deposition of each component can avoid the self-passivation layer formed in the open atmosphere, which might bring in the additional difficulties to understand the interfacial phenomena. There are one magnetron sputtering system (two direct current sputtering guns and two radio-frequency sputtering guns) and one evaporation system (two e-beam sources and two thermal sources) which enable us to deposit a wide range of materials and chemistries, ranged from metal alloys, oxides, nitrides, and polymer coatings. The Li capacity is determined by the film thickness; therefore, this system can be used to study cycle efficiency without the concern of excess Li that is present in the Li foil electrodes reported in most of the literature. In parallel, the PLD system will be used to prepare Li/SE and SE/cathode layered structures as model interface and interphase systems.

To investigate the interfacial mechanical stability, we have prepared three representative systems which have different chemical stability with Li metal and cathodes, including $Li_7La_3Zr_2O_{12}$ (LLZO), $Li_{3x}La_{2/3-x}TiO_3$ (LLTO), and Lithium phosphorous oxy-nitride (LiPON). These SEs paired with the typical cathode materials such as $LiCoO_2$ and NMC, which forms a variety of interphase/interphase, will enable us to investigate how the interphase formation impacts the interface mechanical stability. In addition, by tuning the thickness of Li metal on SE, we can control Li capacity which will be all consumed to form interphase.

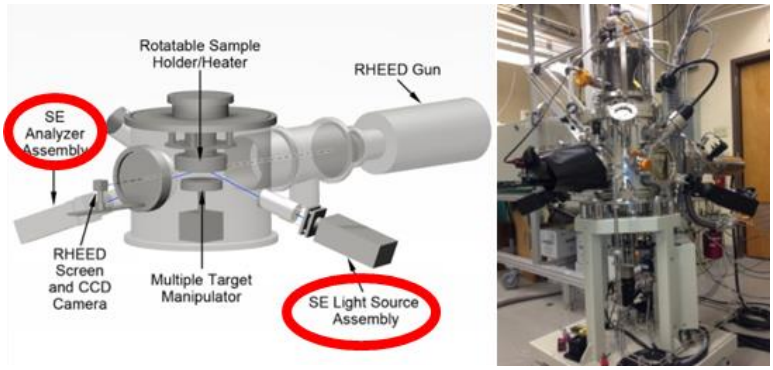

Figure 3. The thin film deposition systems for developing all solid-state battery model systems, including DC/RF sputtering systems and thermal/e-beam evaporation systems which all are integrated inside gloveboxes (above). Pulse laser ablation system (below) is for making thin film cathodes and solid electrolyte.

Figure 4. The in-situ characterization capabilities for fundamentally understanding the coupled mechanical and electrochemical behaviors in all solid-state batteries

Evaluation of the deformation and failure mechanisms of interface/interphase requires knowledge of elastic modulus of individual components associated with a given interface, along with the interfacial fracture strength and toughness. The spatial scale of interface/interphase regions typically is under one micrometer, and thus unique small-scale mechanical characterization techniques are critical to obtain those properties. During the past three years, the team has adopted several in-situ diagnostic tools (**Figure 4**) from previous BMR projects, and also expanded the capability, such as in-situ AFM, XPS, and pressure sensor to deep understand the interfacial mechanical and chemical behaviors in SSB.

4.2 Developed fundamental understanding of stress measurement of solid electrolyte during lithium Plating

During electroplating of lithium metal using garnet-based electrolyte such as $Li_7La_3Zr_2O_{12}$ (LLZO), two types of stress can be generated. First is the stress at the lithium metal/LLZO interface, which arises from inhomogeneous interfacial contact and volume change near the interface, and the electrode-electrolyte reaction layer. Second is the stress from the local defects inside the bulk solid electrolyte, which can cause current amplification and lithium metal penetration. The lithium metal penetration through the solid electrolyte (either bulk or grain boundary) can result in short circuiting, which is one of the main challenges that garnet-based solid electrolyte faces for a real-life application of all solid-state battery.

Both types of stress could make our solid electrolyte sample a measurable bending, which can be detected through multi-beam optical sensor (MOSS). With this measurable bending, we hope to relate the effect of stress on dendrite formation/penetration. Some information we intend to study are: 1) What kind of stress (tensile and compression) does the sample experience during plating at different current density? 2) What is the magnitude of stress experienced in LLZO and/or plated Li metal? 3) What drives the stress build-up in LLZO? To investigate these questions, LLZO

pallet was prepared with reflective coating using e-beam deposition. A thin layer of copper (2um) and gold (50nm) current collectors were deposited directly onto the LLZO pallet to have a reflective surface and was capped with either SiO2 or Al2O3 (50nm) to improve the structural integrity of the current collector during plating. The schematic of the modified sample is shown below in **Figure 5a**.

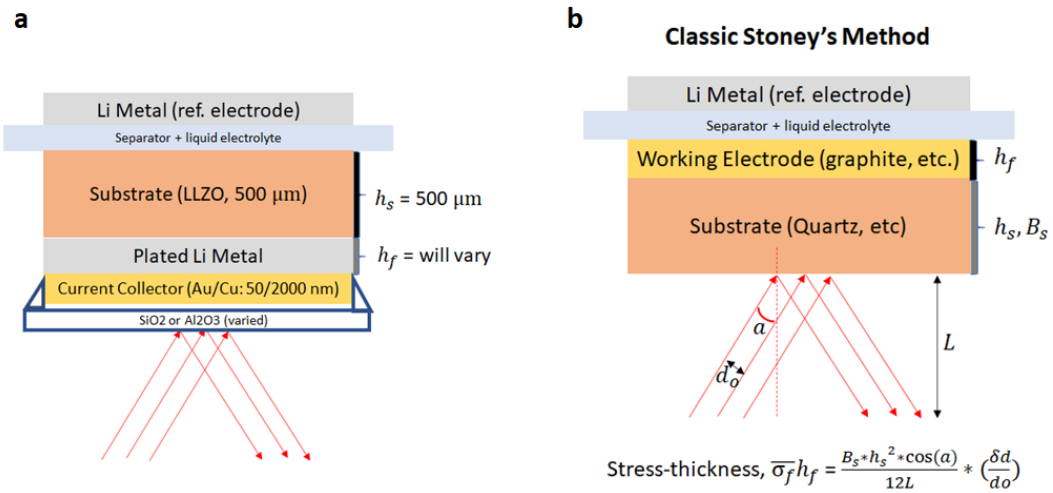

Figure 5. a) Schematic of the MOSS sample using LLZO solid electrolyte with a reflective current collector for bending measurements. b) schematic of traditional MOSS electrode using classical Stoney's equation.

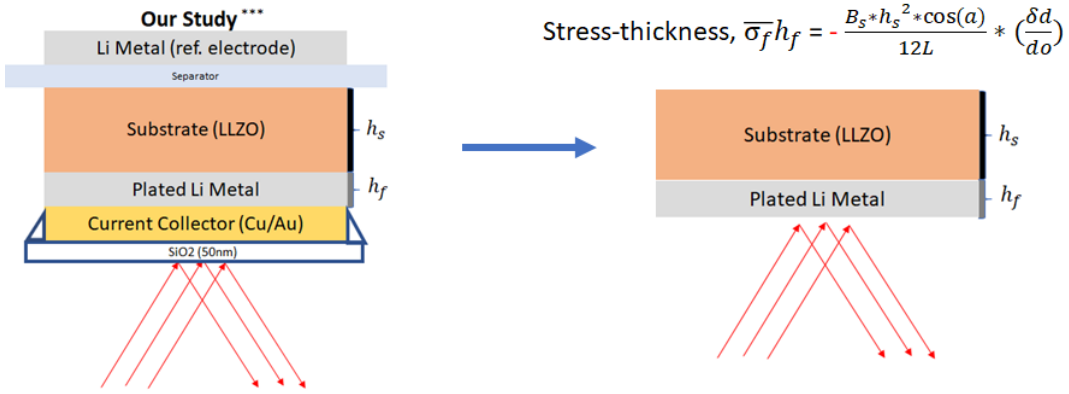

Figure 6. Oversimplified approach of interpreting the bending measurements using LLZO. The resulting stress thickness equation is simply the negative value of classical Stoney's equation.

Lithium metal was used as a reference electrode, along with separator and liquid electrolyte to ensure good contact between lithium metal and the solid electrolyte during bending process. It is important to note that the bending measurement carried out with LLZO solid electrolyte differs from that of conventional electrode configuration used for classical Stoney's equation (**Figure 5b**) to convert bending to stress-thickness. To assess our data accurately, it is essential that modeling work provides a way to interpret out curvature data. As an oversimplified approach (for now), we neglect the contributions from thin reflective current collectors and treat LLZO as the substrate,

and the plated lithium metal as the working electrode. This will result in grossly oversimplified stress-thickness value as shown in **Figure 6**.

Although this interpretation assumes that the stress is only generated by a thin Li film, we can look at these simplified data to determine the general trend of the bending during plating. Nonetheless, the results shown below are not expected to be valid, since the film is not sufficiently thin and there are other likely sources of stress as mentioned above.

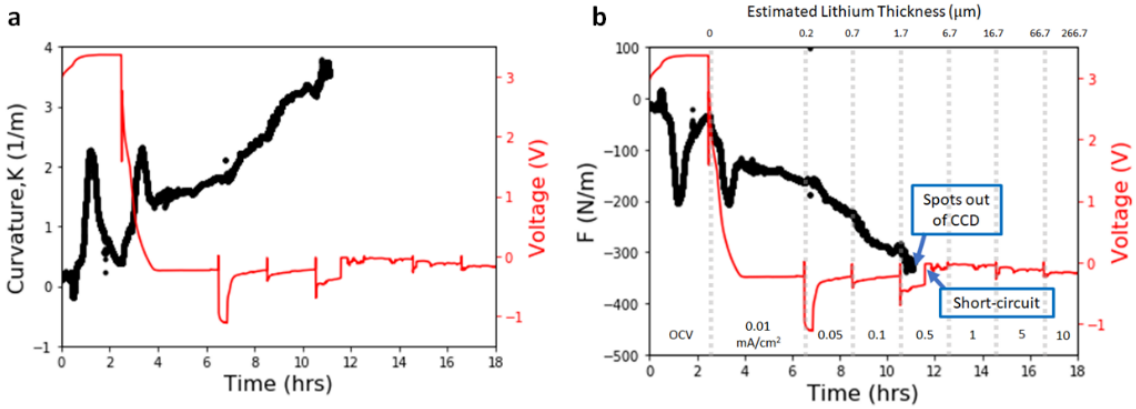

Figure 7. a) Curvature and Voltage vs. Time measured by MOSS using LLZO solid electrolyte. b) Membrane force F and measured voltage vs. Time using oversimplified approach from Eq. (1).

As shown in **Figure 7b**, an increase in compressive stress was observed prior to possible short-circuit feature in voltage profile. The stress values prior to short-circuiting is at around -150 MPa, which will need further analysis to evaluate. This large stress values we observed cannot be explained solely by the growth stress in lithium metal, which was previously reported to be around 0.2 MPa. The stresses we measured that are three orders of magnitude higher than the growth stress in lithium metal are most likely contributed by the stiff solid electrolyte prior to short-circuiting.

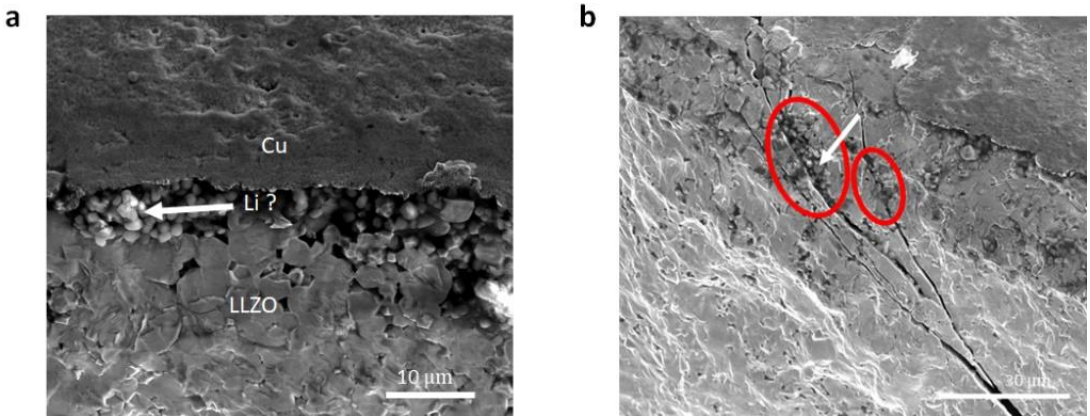

Figure 8. a) Cross-sectional image of a fractured surface (near Cu side) after short circuiting. b) Li metal penetration through the LLZO solid electrolyte along the grain-boundary.

After the short-circuiting event, the LLZO pallet was then fractured and imaged using SEM. As shown in **Figure 8a and 8b**, plating of lithium metal was observed both in Cu/LLZO interface and along the LLZO grain boundary. These post-mortem images will be essential in building the valid model that can describe the bending measurement accurately. A proof-of-concept experiment was carried out to investigate evolving stress when using garnet based LLZO solid electrolyte

during plating. The schematic from Figure 1a using reflective current collectors showed that it is possible to measure curvature associated with stress in LLZO|Li electrode. However, further improvements are required in order to measure the curvature accurately throughout long time of plating. Hence, methods to improve the reflectivity of the LLZO|Li cell is paramount. Hence, a new schematic was carried out to improve the reflectivity of the samples by using a reflective quartz wafer. Details on the improve method and initial sets of measurement is presented.

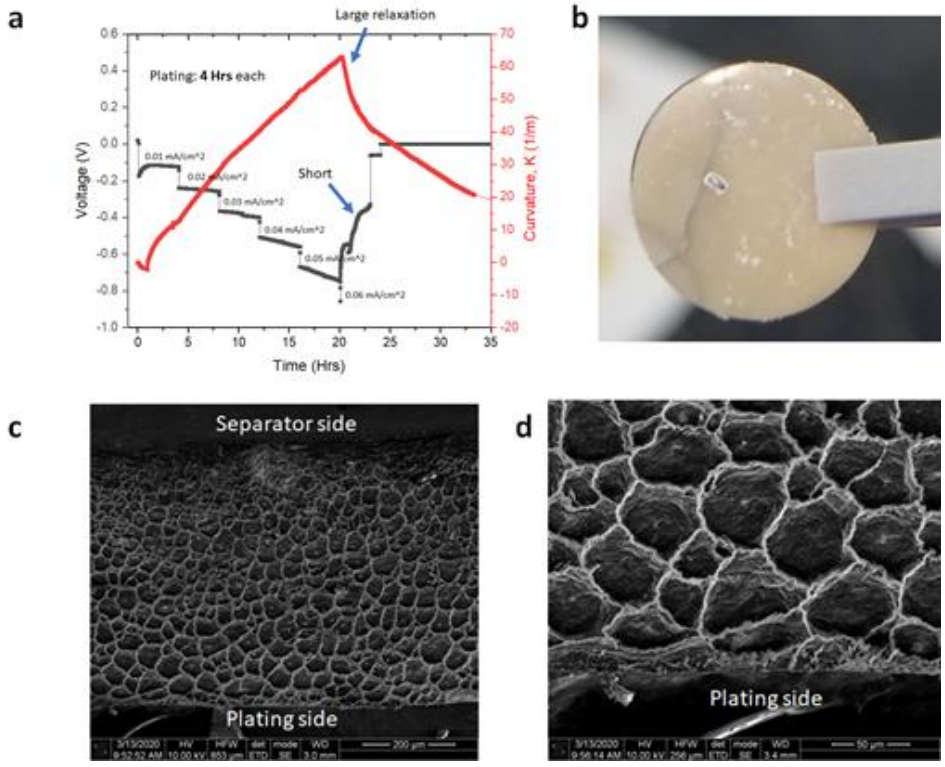

Figure 9. a) Voltage & curvature vs. time of the LLZO/quartz electrode. Black and red lines indicate voltage and curvature profile, respectively. Plating current is applied as a stepwise increase of 0.01 mA/cm2 increments every 4 hours, starting at 0.01 mA/cm2. Both figures show a similar trend of linear increase in curvature prior to short-circuiting. b) Visible crack and fracture on the LLZO pallet after the shorting experiment presented in Figure 8a. c-d) Cross-sectional SEM image of the fracture surface after manually breaking the pallet along the crack.

With new and improved cell, galvanostatic plating was carried out with current density of 0.01 mA/cm^2 with stepwise increase in current density of 0.01 mA/cm^2 increments every 4 hours to correlate curvature evolution with LLZO's shorting phenomena. No stripping sequence was added in this experiment to ensure that the current was unidirectional at all times. The results are shown in **Figure 9a**, which shows a large increase in curvature prior to the short-circuiting event. After either partial or complete short-circuit event has taken place, the curvature shows relaxation in the opposite direction. The curvature relaxation taking place right at the shorting event suggests that the linear increase in curvature during plating is indicative of stress evolved within the solid electrolyte prior to shorting. After the cell has shorted, the electrodes were taken apart in an Ar filled glovebox to for post-mortem imaging. As seen in **Figure 9b**, the shorted pallets exhibit cracks that have propagated through the LLZO pallet. The pallet was mechanically broken apart by applying pressure near the cracks. After the shorting has taken place, **Figure 9c and 9d** indicate

that the crack is propagated via lithium metal plating along the grain boundaries of LLZO, which has been reported in the past. The curvature evolution before and after the shorting phenomena along with our post-mortem images suggest that lithium metal penetration through the solid electrolyte result in a stress build up in the LLZO pallet, which we demonstrate that it is detectable with in-situ curvature measurements.

4.3 Developed in situ nanoindentation technique to investigate the mechanical properties of Lithium Lanthanum Zirconium Oxide (LLZO):

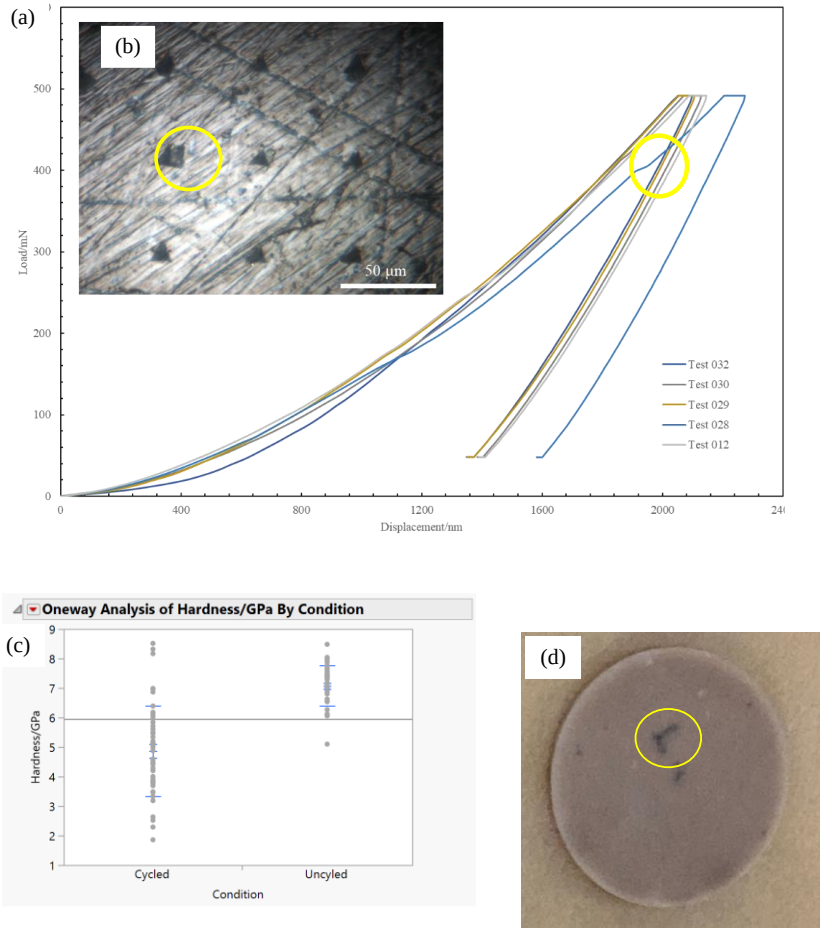

Figure 10. (a) Load vs. Displacement curve for five indents into the uncycled LLZO pellet. (b) Microscope image post indentation of the uncycled LLZO surface, yellow circle highlights the chip in the surface. (c) Histogram results comparing the hardness of cycled vs. uncycled LLZO. (d) Photo of the cycled LLZO sample, dark spot highlighted by a yellow circle.

To help understand the mechanisms responsible for the degradation of the LLZO/electrode interfaces and interphases, we performed nanoindentation measurements on an uncycled and electrochemically cycled Ta doped LLZO pellet. The changes in mechanical properties after cycling may provide insight into these degradation mechanisms. For this initial study, a LLZO sample was placed between two lithium metal electrodes and cycled until failure at GM R&D Center. The failed cell was disassembled and the LLZO pellet was removed for indentation measurements at University of Kentucky. A dark spot was observed on the cycled LLZO pellet,

Figure 10 (d). Because the cell short-circuited, we believe this dark spot contains lithium dendrites. For both samples, fifty indents were made in an array spaced out evenly to obtain a statistical average and to overcome any variation due to surface roughness. For the cycled sample, the array of indents was concentrated overtop of the dark spot. Indents were made to a maximum load of 490 mN then held at maximum load for 10 seconds before unloading. The load *vs*. displacement curves Figure 6(a), were analyzed with the Oliver and Pharr method to extract the average Youngs Modulus and hardness. After using the JMP statistical software to identify and remove any outliers, histograms were created to obtain the mean and standard deviation for both Youngs modulus and hardness. The mean modulus and hardness for uncycled LLZO is 84.3 ± 4.4 GPa and 7.1 ± 0.7 GPa, respectively. For the cycled LLZO, the mean modulus and hardness was 80.2 ± 13.9 GPa and 4.9 ± 1.5 GPa, respectively. Because of the large standard deviation, a statistical significance t-test was performed comparing both the modulus and hardness of cycled *vs*. uncycled LLZO. The confidence level was set at 95%. With this test it was determined that there is no significant difference between the two sample with regards to Youngs modulus. But, as shown in Figure 6(c), there is a significant difference between the hardness.

The decrease in the hardness could be due to the presence of lithium dendrites in the cycled sample. However, the modulus value is affected little because the small volume fraction of the lithium dendrites even in the dark region. In addition, there are "jumps" in the load vs. displacement curves which are commonly associated with cracking or facture of the samples caused by the indenter. A "jump" can be seen in Figure 6(a) on the uncycled LLZO for indent #28 circled in yellow. Post measurement microscope imaging reveals a chip on the surface, **Figure 10(b)** circled in yellow, occurred during indent #28. Further investigation is needed to determine the fracture behavior of uncycled *vs*. cycled LLZO. Future work will also include studying the mechanical behavior of the Li metal electrode. Together, these studies will help reveal the degradation mechanisms at the Li/LLZO interface and/or interphase.

4.4 Investigated the effect of pressure on the interface between lithium lanthanum zirconium oxide (LLZO) and lithium metal electrodes:

The effect of external pressure on the interfacial resistance between Ta doped LLZO solid electrolyte and lithium metal electrodes were investigated using electrochemical impedance spectroscopy (EIS). Prior to electrochemical cycling, a lithium metal symmetric pouch cell was placed in a homemade pressure device. An external pressure of 1.81 MPa was then applied for less than 1 minute, and an EIS measurement was taken to record the contact resistance while under this max pressure. The external pressure was then removed. After removing the pressure, EIS measurements were taken as a function of time to study the cell's response. An intriguing new observation was seen upon removing the external pressure. The interfacial resistance continued to decrease even without the driving force of stack pressure. As seen in **Figure 11**, the interfacial resistance decreases over the course of 7 days after the initial pressure of 1.81 MPa was removed.

We propose that after the pressure is removed, the interfacial resistance decreased further as a result of the power-law creep of lithium metal which increased its contact area with the LLZTO as schematically shown in **Figure 12**. The dislocations formed during the initial application of pressure and start to move once pressure in removed because of the back-stress in the dislocation substructures.[2] The dislocations find their way to the surface, reducing stress and creating more contact area with LLZTO. In addition to the driving force due to creep, growing the contact area between lithium and LLZTO is energetically favorable since LLZTO is lithiophilic.[3-5] We propose that the lithium metal continues to flow even after the pressure is removed to reduce

surface energy of lithium metal and LLZTO, as well as the strain energy in the dislocation substructure. However, this proposal should be examined in the future.

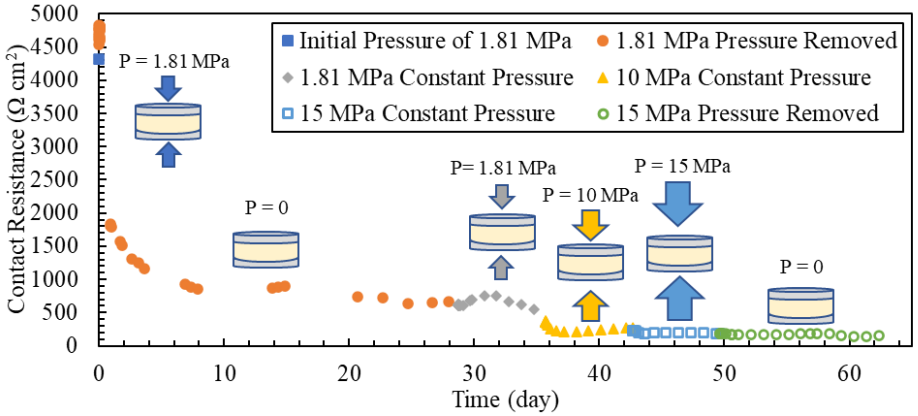

Figure 11. Contact resistance vs. time plotted out under various pressure conditions. The initial pressure of 1.81 MPa was applied at time zero.

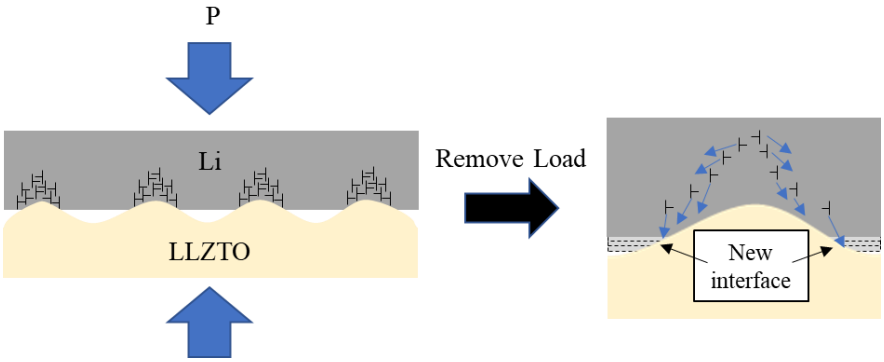

Figure 12. Conceptual diagrams depicting the cross section of lithium and LLZZTO interface. The formation of dislocation substructures, and the movement of dislocations after removing the external pressure causing an increase in the contact area with LLZTO.

4.5 Explored the relationships between interfacial mechanical failure mechanisms and current density and pressure.

Optical spectroscopic ellipsometry measurements were conducted in the photon energy range of 1.2 – 5.9 eV on a lithium foil sample; its surface was prepared to a mirror-like finish before being transferred into the vacuum chamber for measurements. Experiments were conducted first in vacuum (i.e., ~10^{-7} Torr) before exposing the lithium to air. Measurements were taken every minute for 10 minutes to observe how the surface of lithium changed with exposure time. Analysis and modeling of the raw data, shown in **Figure 13(a),** indicates a surface layer is present upon initial testing, about 40 nm thick. As seen in **Figure 13(b),** this layer starts to quickly grow after 1 minute of exposure to air, then the rate of growth slowly decreases with time around 5 minutes. Although visually lithium looked very shiny and clean, a surface layer did exist on the lithium foil, which should be taken into consideration when studying lithium metal. This experimental result and analysis provide a baseline for future work studying the interface and interphase of lithium with materials such as solid electrolytes.

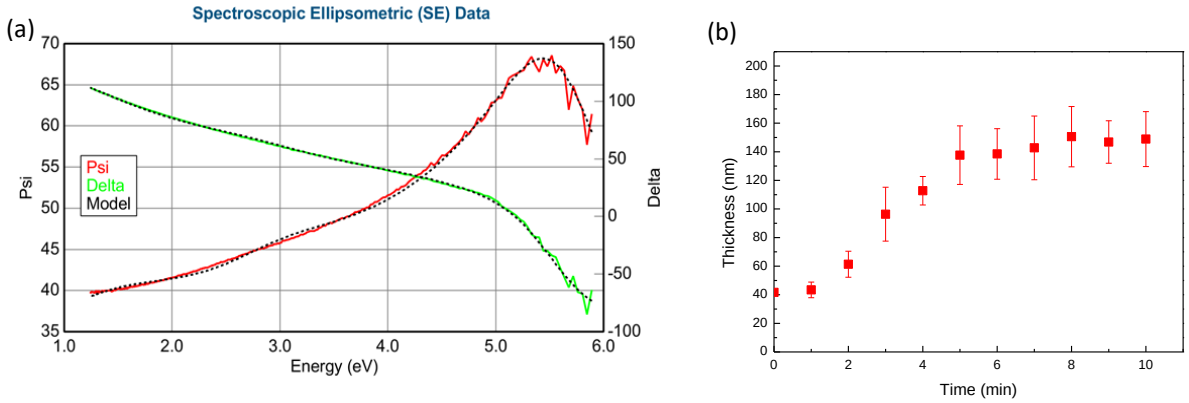

Figure 13. Optical spectroscopic ellipsometry measurements and modeling of lithium metal (a) Psi and Delta vs. Energy. (b) Estimated surface layer thickness increasing in air exposure.

4.5.1 The energetics of Li vacancy formation and diffusion near a Li/SEI interface based on DFT calculations

Electroplating has been the main focus in mitigating the dendrite growth on Li-metal electrode; however, the stripping process is as critical, since the non-smooth Li surface during stripping will leads to non-uniform local current density, planting the seeds for dendrite growth. This year, we combined density functional theory (DFT) and Kinetic Monte Carlo (KMC) simulations to investigate the vacancy evolution in Li interfaced with different SEI/coating materials. It was found that lithiophilic interface, such as Li/Li_2O, repels vacancies into the bulk Li, so Li can quickly fill the Li vacancies near the Li/Li_2O interface and maintain a smooth Li surface. In contrast, lithiophobic interface, such as Li/LiF, traps Li vacancies toward the interface and the accumulated Li vacancies form voids and roughen the surface. The predicted critical stripping current density, below which a smooth Li surface will be maintained, is therefore much faster at the lithiophilic Li/Li_2O interface than that at the lithiophobic Li/LiF interface. It was further revealed that the lithiophilicity at different SEI or coating materials can be ranked as Li/Li_2O > Li/LiPON > Li/Li_2CO_3 > Li/LiF based on the calculated interfacial adhesion and accumulation of electron density at the interface. This suggests that interface and coating design can be effective for maintaining a smooth Li surface during stripping process, another challenge to achieve a dendrite-free Li-metal electrode in both liquid and solid electrolytes.

Figure 14a and **14b** shows the relaxed structures of Li(001)/LiF(001) and Li(001)/Li_2O(110) interfaces, which have the lowest interfacial formation energies compared to other orientations.[31,34] About 75% and 56% surface lithium atoms form direct bond (a bond length less than 2.2Å) with the O and F anions on the Li_2O and LiF surfaces, respectively. **Fig. 14c** and **14d** show the vacancies formation and migration energies near the interface, especially in the first four layers (L1-L4) and reveal the vacancy interaction with the interface. The red dots are the DFT calculated vacancy formation energy profiles at each layer. The vacancy formation for bonded Li atoms is the highest at the Li/Li_2O interface but the lowest at Li/LiF interface (Figure 8c and 8d). For the unbonded Li atoms, the Li vacancy formation becomes more possible at the Li/Li_2O interface, while is even more possible at the Li/LiF interface. This means, Li/Li_2O interface tends to repel Li vacancy, while Li/LiF interface attracts Li vacancy. The vacancy formation energies drop quickly from the interface to the bulk values. The black lines (connecting the red and blue solid circles based on DFT with NEB calculations) in Fig. 8c and 8d show the energy landscape during Li vacancy migration. It can be revealed that once a vacancy is present at the interface (due

to the stripping), the vacancy is likely to migrate toward the bulk Li metal due to the repulsion in the Li/Li_2O interface, while is likely to be trapped at the Li/LiF interface, as the Li/LiF interface attracts Li vacancies.

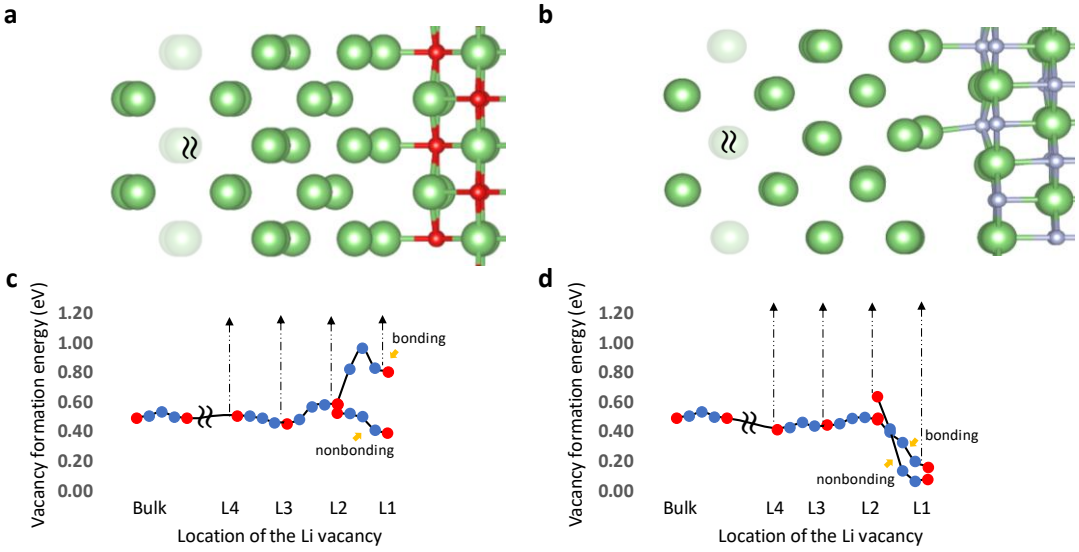

Figure 14. Relaxed interfaces and the Li vacancy migration landscape. Sideview of the relaxed interfaces (partially shown) of (a) Li(001)/Li_2O(110) and (b) Li(001)/LiF(001) interfaces. Vacancy formation energy profile and migration landscape for bonded Li atoms and non-bonded Li atoms at the interfaces of (c) Li(001)/Li_2O(110) and (d) Li(001)/LiF(001) interfaces. Solid red circles represent the vacancy formation energy and solid blue circles represents Li diffusion path based on NEB technique. Note the diffusion of Li atom and Li vacancy is reverse (O in red, Li in green, and F in grey).

4.5.2 Vacancy accumulation and diffusion at different Li/SEI interfaces

KMC simulations with the rate constants computed from DFT calculated energy barriers were used to test if the diffusion process will fill the surface vacancies and maintain surface smoothness. In the beginning of the simulation, 23-25% Li atoms within the first two layers (L1-L2) were removed randomly (**Figure 15b and 15c**), mimicking an initial surface state created by stripping. **Figure 15a** plots the average distance of the vacancies from the interface and how it changes with KMC time. The vacancies at the Li/Li_2O interface quickly move away from the interface after $8.43x10^{-11}$ s, while in Li/LiF the vacancies barely move even after $1.60x10^{-06}$ s. **Figure 15d** further compares the distribution of vacancies after 10^5 KMC steps to the initial condition. For the Li/Li_2O interface, only 16% of the vacancies are at the interfaces, while 80% are distributed uniformly inside of the Li (**Figure 15e**). For Li/LiF, the vacancies stay at the interface and connected to voids as shown in the final structures (**Figure 15f**). The timestep in KMC model depends on the frequency of occurring events. In the Li/L_2O interface, the main events are the diffusion of Li vacancies, which occurs at a high frequency. In the Li/LiF interface, after the vacancies trapped at the interface, diffusion become a rare event, so the KMC step has a longer time span. This confirms that Li can fill the vacancies at the Li/Li_2O interface very quickly and reveals that this interface can withstand a higher current density without the presence of voids.

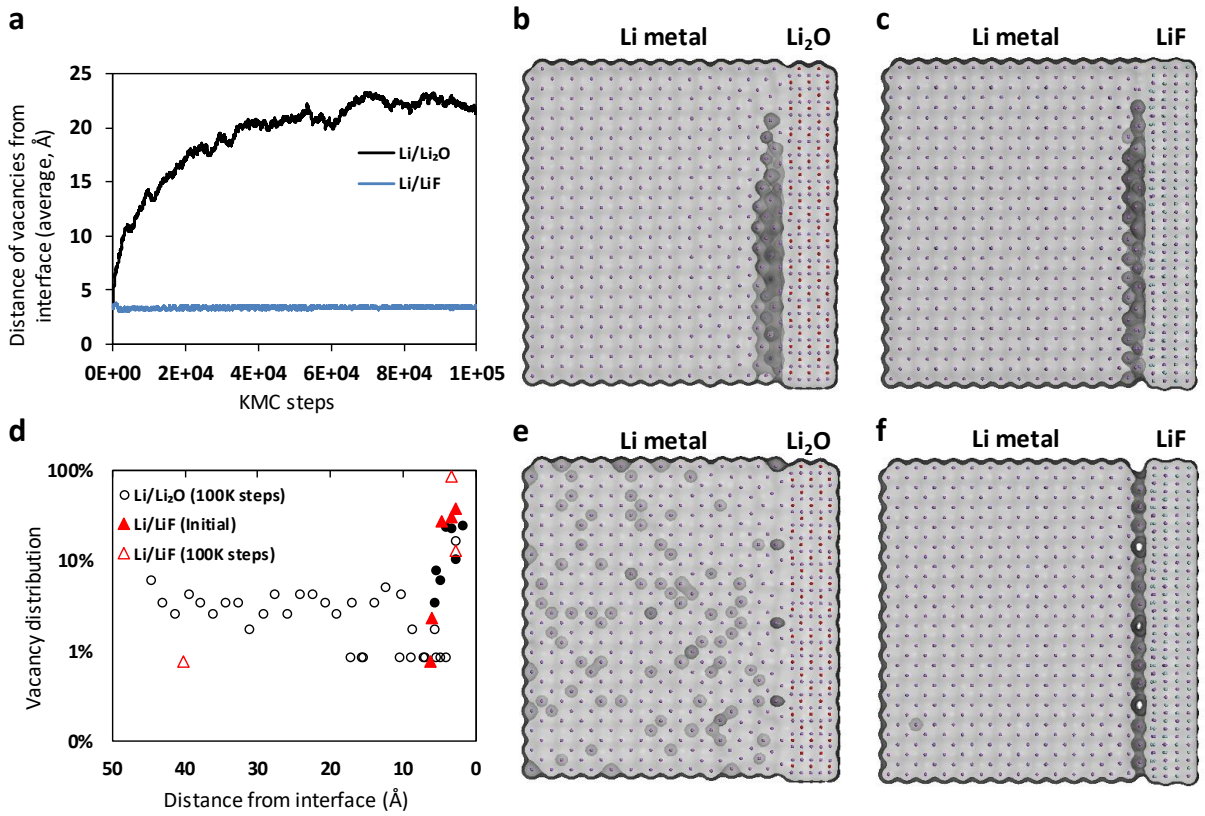

Figure 15. KMC simulation of the vacancy evolution in the presence of interfacial vacancies at Li/Li_2O and Li/LiF interfaces. (a) The average distance of the vacancies from the interface variation versus KMC steps. The initial structures of (b) Li/Li_2O and (c) Li/LiF interfaces with vacancies on Li surface. (d) The vacancy distribution in the Li slab in the beginning and at 10^5 KMC steps. The final structures (at 10^5 KMC steps) of (e) Li/Li_2O at time of 8.43×10^{-11}s and (f) Li/LiF at time of 1.60×10^{-06} s.

4.5.3 Development of the analytical model to predict the CCD for Li/SE interfaces

The combined impacts of the interface and compressive stress (stack pressure) on the Li surface morphology are considered to predict the critical current density (CCD) at the Li/solid electrolyte (SE) interface during the stripping process. To take these two impacts into consideration in an analytical model, the Li flux contributed by the vacancy hopping and creep effects should be quantified. The representative Li/Li_2O (lithiophilic), Li/LiF (lithiophobic) and the experimentally intensively studied Li/LLZO interfaces are chosen to justify this model.

The flux due to hopping is calculated based on the hopping rates, which are obtained from DFT calculated hopping barriers. Considering three consecutive Li layers $(j-1, j, j+1)$, the hopping flux across the jth layer $(\frac{dN_j}{dt})$ is defined as

$$\frac{dN_j}{dt} = \frac{1}{2}k_{f,j+1}(N_{j+1} - N_j) - \frac{1}{2}k_{f,j}(N_j - N_{j-1}) - \frac{1}{2}k_{b,j}(N_j - N_{j+1}) + \frac{1}{2}k_{b,j-1}(N_{j-1} - N_j), \quad (1)$$

where $k_{f,i}$ is the forward hopping rate, $k_{b,i}$ is the backward hopping rate and N_i is the number of Li atoms on the ith Li layer $(i = j-1, j, j+1)$.

Since Li atoms are stripped from the Li surface (the first layer), the hopping flux on the first layer is

$$\frac{dN_1}{dt} = \frac{1}{2}k_{f,2}(N_2 - N_1) - \frac{1}{2}k_{b,1}(N_1 - N_2). \quad (2)$$

When hopping can catch up with the vacancies generated during stripping, the concentration on the first layer does not change, which requires that

$$\frac{dN_1}{dt} = \frac{1}{2}k_{f,2}(N_2 - N_1) - \frac{1}{2}k_{b,1}(N_1 - N_2) - k_s N_1 = 0, \quad (3)$$

where k_s is the stripping rate applied on a unit area. When the forward and backward hopping events are symmetric ($k_{f,2} = k_{b,1}$), Eqn. (3) becomes

$$\frac{dN_1}{dt} = k_{f,2}(N_2 - N_1) - k_s N_1 = 0. \quad (4)$$

Then the stripping rate is related to the hopping rates according to

$$k_s = \frac{k_{f,2}(N_2 - N_1)}{N_1} = k_{f,2}\Delta N / N_1, \quad (5)$$

where $\Delta N = N_2 - N_1$. Because the current density is defined as current per unit area, the critical current density (i_c) is calculated using

$$i_c = \frac{qk_s}{A_0} = \frac{qk_{f,2}}{A_0} * \frac{\Delta N}{N_1}, \quad (6)$$

where q is the electric charge of an electron and A_0 is the unit area on the Li (001) plane. The backward hopping events always happen, and the stripping is more related to the forward hopping, therefore, Eqn. (6) can be used to predict the CCD at any Li/SE interface when the forward hopping rates from the second layer to the first layer ($k_{f,2}$) are available. It should be mentioned that Eqn. (6) holds in a short time (dt), which requires $\frac{\Delta N}{N_1}$ is small.

The creep induced flux ($\dot{n_p}$) over a unit area is a function of the applied strain rate ($\dot{\varepsilon}$) according to

$$\dot{n_p} = \frac{N_A A_0 L \dot{\varepsilon}}{V_{Li}}, \quad (7)$$

where N_A is the Avogadro's constant, L is the thickness of the Li metal and V_{Li} is the molar volume of Li. The strain rate ($\dot{\varepsilon}$) is a function of the stack pressure (σ) and the temperature (T)

$$\dot{\varepsilon} = \sigma^m A_c \exp\left(-\frac{Q_c}{RT}\right), \quad (8)$$

where m, $A_c$and Q_c are constants measured from experiments (LePage et al, 2019, A89) and R is the gas constant. Combining Eqn. (7) and (8), $\dot{n_p}$ is expressed as a function of L, σ and T using

$$\dot{n_p} = \frac{N_A A_0 L}{V_{Li}} \sigma^m A_c \exp\left(-\frac{Q_c}{RT}\right). \quad (9)$$

Since the polynomial effect of σ ($m = 6.6$) is more prominent than the effects of L and T on $\dot{n_p}$, L ($L = 100\ \mu m$) and T ($T = 298\ K$) are treated as constants and thus $\dot{n_p}$ is only dependent on the applied stack pressure. When both the hopping flux and the creep induced flux are considered, i_c is expressed as

$$i_c = \frac{qk_s}{A_0} = \frac{q(k_{f,2} + \dot{n_p})}{A_0} * \frac{\Delta N}{N_1}. \quad (10)$$

4.5.4 Prediction of critical current densities for Li/Li$_2$O, Li/LiF and Li/LLZO interfaces using the analytical model.

Table 1 lists the CCD ($\frac{\Delta N}{N_1} = 10^{-6}$) predicted for Li/Li$_2$O, Li/LiF and Li/LLZO interfaces. The predicted CCD here are consistent with our previous KMC simulations considering the hopping events for Li/Li$_2$O and Li/LiF. Although the CCD for LLZO is higher than the experimental values by 2 orders of magnitude, the LLZO surface in experiments is normally covered with some Li_2CO_3 (not a flat surface), which limits the measured CCD.

Figure 16 shows i_c at different stack pressure for Li/Li_2O, Li/LiF and Li/LLZO interfaces using Eqn. (10) assuming $\frac{\Delta N}{N_1} = 10^{-6}$. For the lithiophilic Li/Li_2O interface (wetting angle 0°), no stack pressure is required to reach a current density of 10 mA/cm^2. In contrast, for the lithiophobic Li/LiF interface (wetting angle 108.7°), a stack pressure around 4 MPa is necessary to achieve the goal of 10 mA/cm^2. For another lithiophilic interface (Li/LLZO, wetting angle 60.2°), the stack pressure is not necessary to reach a stripping current density of 10 mA/cm^2. As the Li/LLZO is not as lithiophilic as the Li/Li_2O, the CCD is smaller than that of the Li/Li_2O interface but larger than that of the Li/LiF interface, suggesting that the analytical model captures the trends of CCD among different Li/SE interfaces.

Table 1. $k_{f,2}$ and predicted CCD for Li/Li_2O, Li/LiF and Li/LLZO interfaces without the creep effects.

	Li_2O	LiF	LLZO
$k_{f,2}$ (s^{-1})	3.31e10	3.76e3	2.14e8
CCD (A/cm^2)	43.0	4.88e-6	0.277

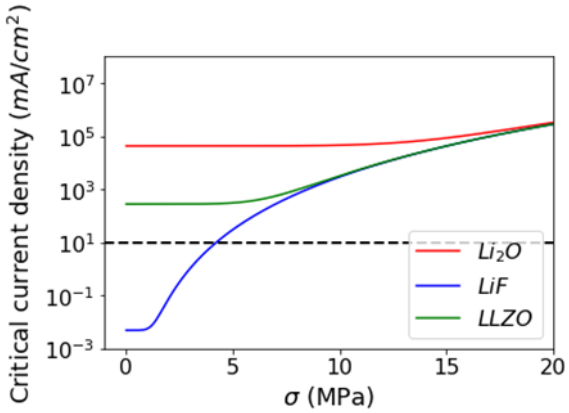

Figure 16. Predicted critical current density at different stack pressures for Li/Li_2O, Li/LiF and Li/LLZO interfaces considering Li hopping and creep induced Li flux.

4.5.5 The critical delithiation current density to maintain a smooth Li surface

To evaluate how the surface roughness of Li electrode (vacancies formed and migrated) is impacted by the two different interfaces under the competition between Li diffusion and the stripping process, the stripping process was then incorporated in the KMC simulation. The stripping mechanism is mimicked by removing Li atoms from the lithium surface layer (L1) with a stripping rate (k_s), and the Li atoms in the SEI were removed to act as an infinite Li atom sink. Removing ~8 atomic layers in the Li-metal in one second (k_s~8 1/s) corresponds to a stripping current density of 1.0 mA/cm^2, which is a typical current density used in experiments.

The vacancy distribution as well as the surface roughness of the Li metal under the stripping current density (simulated by different $k_s$values) in the range of 10^{-6} – 10^3 A/cm^2 for both interfaces. At the typical current density of 10^{-3} A/cm^2 the interface of Li/Li_2O has no vacancies, but the accumulation of the vacancies can be clearly seen at the Li/LiF interface (41 vacancies at L1 out of 42 delithiated Li). When the current density increased to 10^1 ~10^2 A/cm^2 (**Figure 17a and 17b**, respectively), the Li/Li_2O interface shows a transition from a smooth Li

surface at 10^1 A/cm^2 with vacancies in the bulk to some trapped surface vacancies (3 vacancies at L1 out of 7 delithiated Li) at 10^2 A/cm^2. The faster stripping rate of 10^2 A/cm^2 is comparable to the Li atom toward the Li/Li_2O interface, so the vacancy filling events are limited. On the other hand, the accumulation of the vacancies at the Li/LiF interface at the of 10^{-3} A/cm^2 gradually disappear as the stripping rates decrease to 10^{-5} ~ 10^{-4} A/cm^2 (**Figure 17c and 17d**, respectively). This means a critical current density (J_C), beyond which vacancies accumulate on the surface of Li, can be defined. To maintain a smooth Li surface, the applied stripping current density should be lower than the J_C which is material and interface sensitive. The simulation results seem to suggest J_C is on the order of 10~100 A/cm^2 and 0.01~0.1 mA/cm^2 for Li/Li_2O and Li/LiF, respectively. Kasemchainan reported the critical stripping current density, J_C, of 0.2 ~ 1.0 mAcm^{-2} under compression pressure for Li/Li_6PS_5Cl solid state cell.[Error! Reference source not found.] Without the compression pressure, the J_C values will be even lower. Thus, the predicted limiting current of Li/LiF interface is on the similar order of magnitude. If the J_C is on the order of 10~100 mA/cm^2 for Li/Li_2O, this stripping (discharge) current density will no longer a limiting factor for Li-metal applications. However, the current model assumes the interface is extremely flat, which is unlikely if the Li_2O is formed by oxidation of Li.

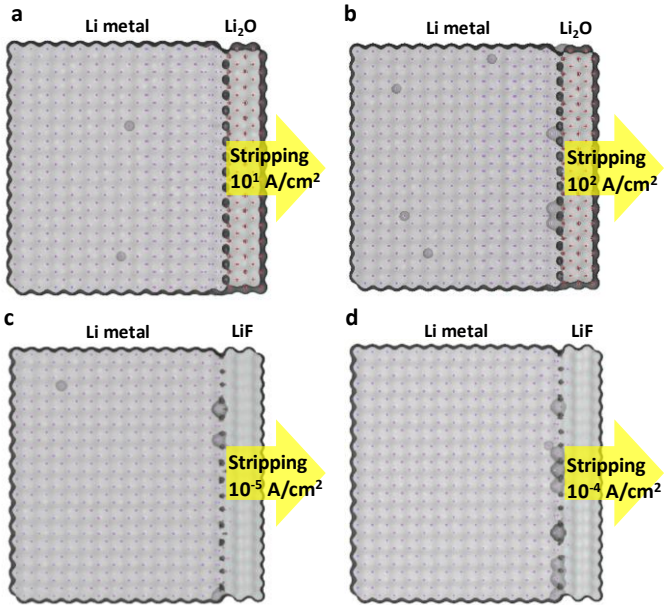

Figure 17. KMC simulation, incorporating the stripping process and the Li atom diffusion, of the formation and evolution of vacancies near the interfaces at different current densities. Li/Li_2O: final structures upon current density at (a)10^1 and (b)10^2 A/cm^2 after 10^5 KMC steps, corresponding to the time at 1.59x10^{-8} and 1.23x10^{-8}s, respectively. Li/LiF: final structures upon current density current density at (c)10^{-5} and (d)10^{-4} A/cm^2 at 10^5 KMC steps corresponding to the time at 1.6x10^{-1} and 2.96x10^{-2}s. Note the numbers of stripped Li atoms in a-d are 3, 7, 5, and 13, respectively, during the simulation time.

4.5.6 Interface Design based on the electronic origin of Coating Materials

Since J_C is interface sensitive, KMC models further revealed that reducing $\Delta E_{2\to1}$ plays a major role in facilitating the void filling at the interface, since more vacancies migrated toward the bulk region. Therefore, it is important to find coating materials that repel Li vacancy away the interface and reduce the energy barrier for Li to move toward the interface, which can be evaluated based on DFT computable interfacial properties. The work of separation of Li(001)/Li_2O(110) is

1.11 J/m^2, and is 0.28 J/m^2 for Li/LiF. Therefore, Li/Li_2O is lithiophilic and Li/LiF is lithiophobic. Understanding bonding nature and the electronic structures of these interfaces will help to guide our coating material design to maintain a smooth Li surface with high critical current density. A simple rationalization to explain the difference of Li/Li_2O and Li/LiF interface is that the Li_2O(110) surface exposes two-lithium under-coordinated O atoms and LiF(001) surface exposes one-Li under-coordinated F atoms. Although both have developed direct Li-O and Li-F bonds after interface relaxation, some O atoms of Li_2O(110) are still undercoordinated, so it can attract more Li, thus is lithiophilic. To quantify the bonding characteristics, the electronic structure origin of the lithiophilic and lithiophobic surfaces was analyzed. The (planar) charge density difference (CDD) was studied (**Figure 18**). The electron density transferred from SEI materials to the interfaces, and more electron density accumulates at the Li/Li_2O interface than that at the Li/LiF interface. This enhanced electron density can attract more Li toward the interface, making Li/Li_2O interface lithiophilic, as well as creating a stronger interfacial adhesion.

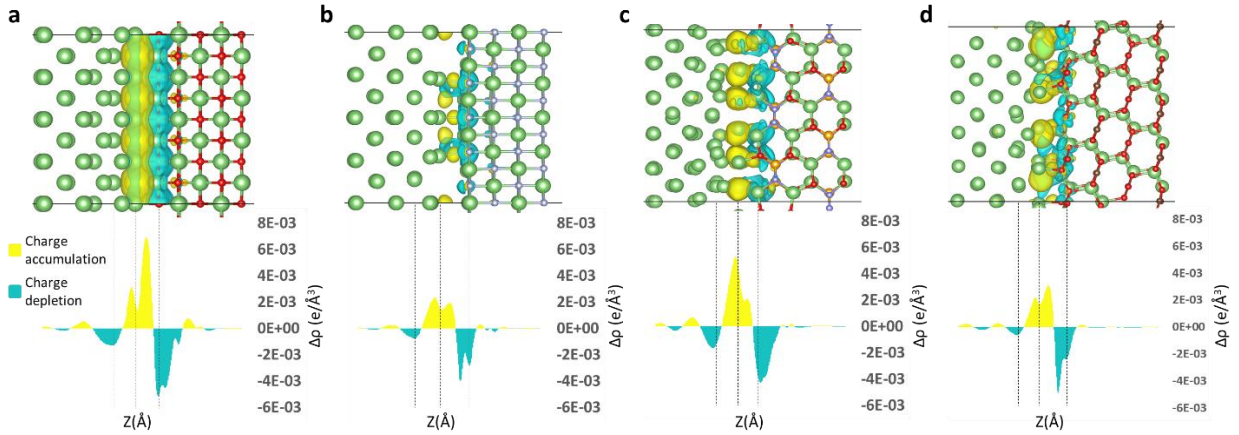

Figure 18. Charge density difference (upper panel) and planar-averaged charge density difference (lower panel). (a)Li/Li_2O, (b)Li/LiF, (c) Li(001)/Li_2PO_2N(010) and (d) Li(001)/Li_2CO_3(001) (O in red, Li in green, F in grey, C in brown, N in light blue, and S in orange).

4.6 Investigation of different polymer nanocomposite-based interlayers to reduce the interfacial resistance of solid-state batteries.

With the help of interfacial coating, the above problems can be eliminated, and the performance can be improved. Here, a mixture composed by three materials is used to coat lithium metal, which includes $LiNO_3$, 1,2-Dimethoxyethane (DME), Trimethyl phosphate (TMP). $LiNO_3$ is a well-known additive in liquid electrolyte and TMP promotes the solubility of $LiNO_3$ in DME. Li_3PO_4 is formed by reduction reaction between lithium metal and TMP.

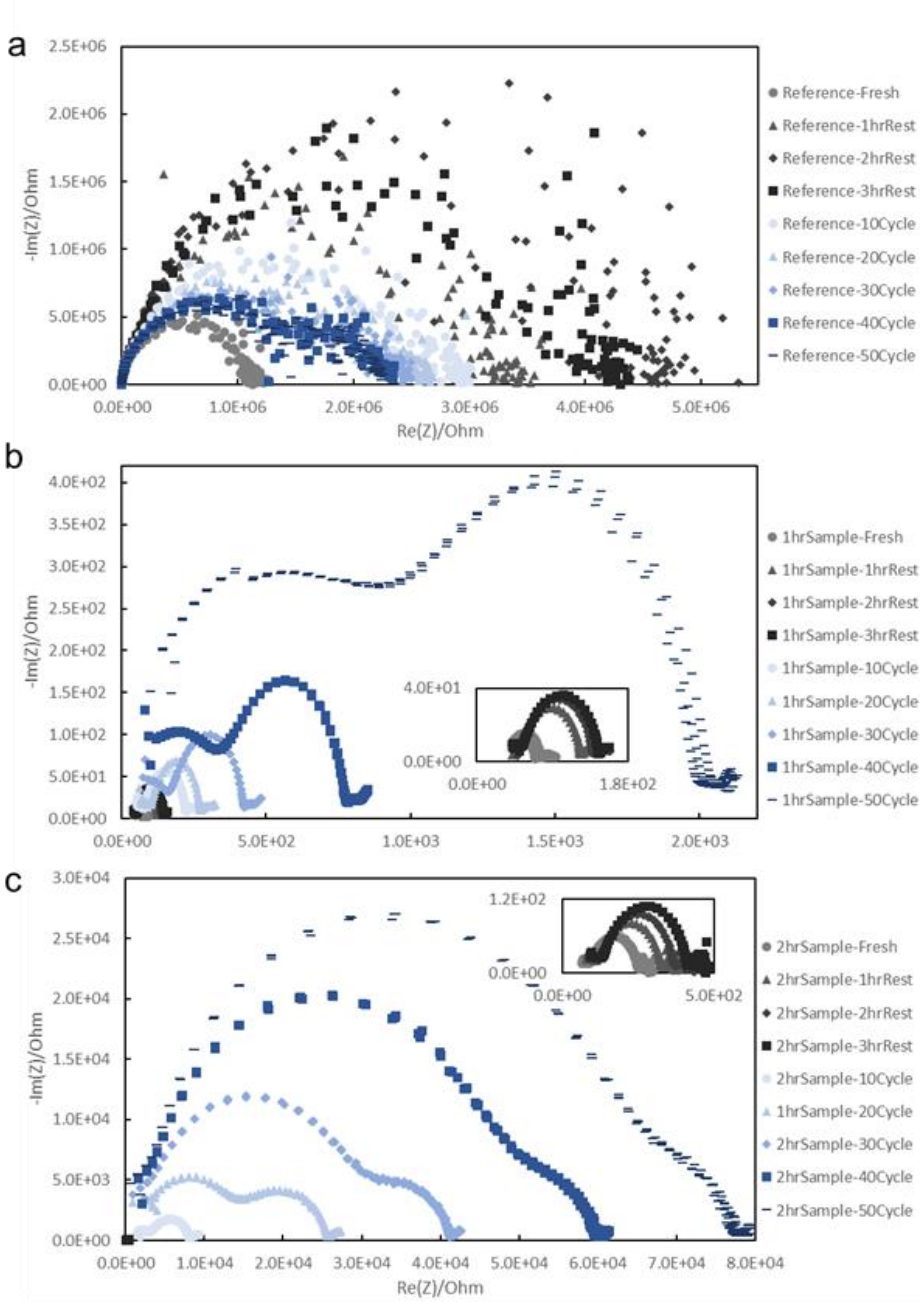

Figure 19. Impedance and cycle performance of reference, 1hr_Sample and 2hr_Sample. (a-c) Impedance increase during 3hr_Rest and 50_Cycle.

As a result, the coating layer composed by Li_3PO_4 and $LiNO_3$ is formed and the interfacial properties are improved when utilizing the coated lithium metal with solid-state electrolyte. LAGP is short for $Li_{1.5}Al_{0.5}Ge_{1.5}(PO_4)_3$ and it possesses a lithium ion conductivity of $5x10^{-4}$ S/cm at room temperature. However, the Ge is easily reduced by lithium metal and this reaction is not self-limiting since the side-reaction product is a mixed electronic and ionic conductive phase. The

impedance and cycle performance are shown in **Figure 19**. Reference LAGP has an initial high impedance of $1*10^6\Omega$, and the impedance is increased by 4 times after 3hrs' rest, indicating an instant chemical side reaction when LAGP contacts with lithium metal. Due to the high impedance, the 1V cut-off voltage is reached instantly after 5μA current is applied. 1hr_Sample has an initial low impedance of 70Ω, which is a substantial improvement compared with the reference. During the 3hrs' rest, the impedance is increased into 146Ω. After 50 cycles, the impedance is increased to 2,000Ω and the overpotential is less than 0.15V. 2hr_Sample has an initial impedance of 250Ω, which is also an improvement compared with the reference. During the 3hr's rest, the impedance is increased into 410Ω. After 50 cycles, the impedance is increased to 78,000Ω and the overpotential is around 0.45V. Among 1hr_Sample and 2hr_Sample, 1h_Sample has the best protection and it improved the cycle stability between lithium metal and LAGP significantly.

4.6.1 Micro-CT to understand the interface reaction between solid electrolyte and Li metal

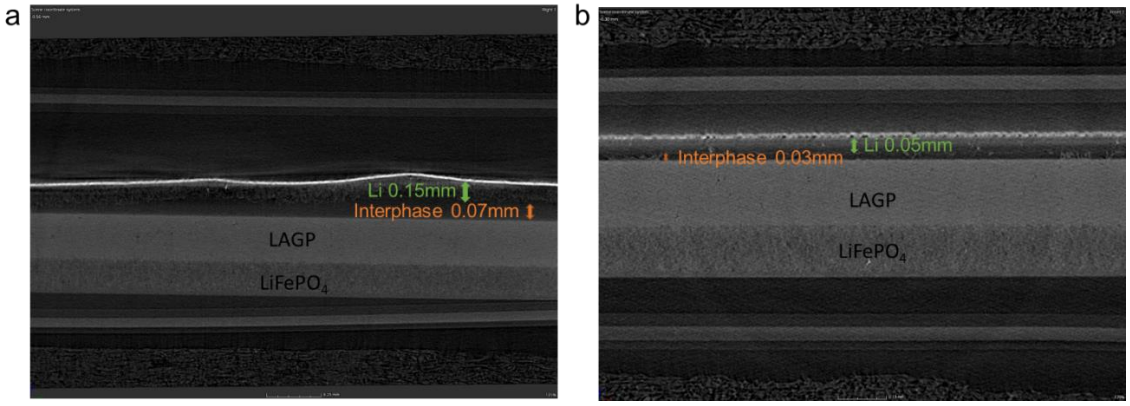

Figure 20: CT scan of the cross-section of Li/LAGP/$LiFePO_4$ cell. (a) Li/LAGP/$LiFePO_4$ cell with control lithium electrode. (b) Li/LAGP/$LiFePO_4$ cell with coated lithium electrode.

LAGP possesses a lithium ion conductivity of $5x10^{-4}$ S/cm at room temperature. However, the Ge is easily reduced by lithium metal and this reaction is not self-limiting since the side-reaction product is a mixed electronic and ionic conductive phase. A computerized tomography (CT) scan can construct a three-dimensional (3D) image of the object non-destructively. Without any air exposure, the interfacial property of the solid-state cell is revealed. As shown in **Figure 20**, the coated sample shows a much stable interphase. The control lithium electrode shows a bumpy structure while the coated lithium electrode is flat. In addition, the control lithium has a thickness around 0.15 mm, which is a three-time increase compared with pristine lithium metal (0.05 mm). As a contrast, the coated lithium still maintains the same thickness as before. The increased thickness of control lithium electrode can be either caused by the unintimate solid-solid contact or the side reaction occurred within the lithium foil. An interphase with a distinct dark color is formed between solid state electrolyte (LAGP) and lithium electrode, and this thickness can directly represent the side reaction level. In the control lithium electrode, the interphase layer caused by the side reaction is 0.07 mm, which is 2.33 times higher than the coated sample (0.03 mm). As a

result, with coating, the side reaction between lithium electrode and LAGP is largely depressed and a good cycle life is reached.

Recently, we have developed a polymer nanocomposite as the interlayer to maximize the interfacial contact between lithium metal and solid electrolyte, therefore, to facilitate the ion transport through the interface. We first deposited a thin film on Li-metal surface by soaking it in DTL solution, which stands for (1,2-dimethoxyethane (DME) solvent with trimethyl phosphate (TMP) and $LiNO_3$ additives). In addition, we also replaced DME with DOL (1,3-Dioxolane) for form more flexible coating. The electrochemical impedance spectroscopy shows the interlayer can significantly reduce the impedance by almost two orders of magnitude, as shown in **Figure 21.**

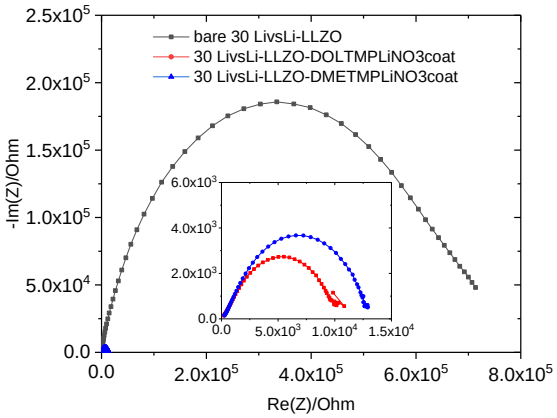

Figure 21. The comparison of interfacial impedance of Li vs. LLZO with different interlayers.

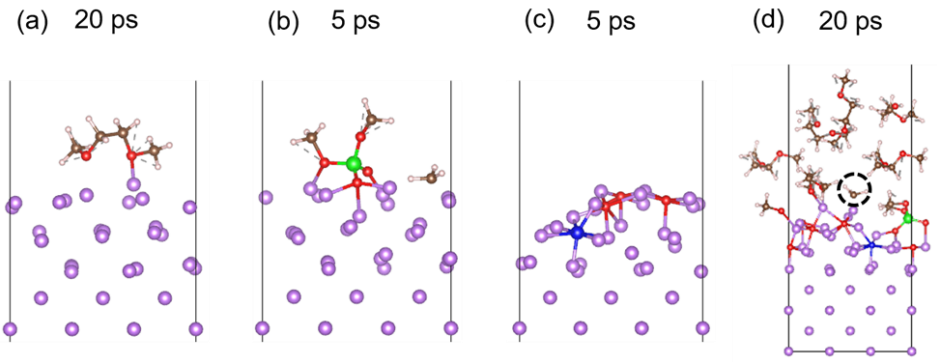

Figure 22 Structures after AIMD simulations. (a) DME molecule (b) TMP molecule, (c) LiNO3 molecule, and (d) DTL solution on the Li metal. Purple: Li, Brown: C, White: H, Red: O, Blue: N, Green: P. The colors for different elements are consistent in all the figures

To correlate the battery performance and the components and properties of the coating layer formed in the soaking process, Density Functional Theory (DFT)-based molecular dynamics (AIMD) simulations together with experimental investigation were performed to study the reaction mechanism of the DTL solution on Li metal surface. When constructing the structures for Li metals covered by the DTL solution, to resemble the 0.8 M $LiNO_3$ in DME/TMP (volume ratio = 5:1) solution in the experiment, 6 DME molecules, 1 TMP molecule and 1 $LiNO_3$ molecule were packed as the liquid solution, relaxed, and formed an interface with Li (001) surface. The AIMD simulation using the NVT ensemble was performed at 400 K with the Nose-Hoover thermostat.

The higher temperature (below the Li melting point, 454 K) was used to accelerate the calculations. The system was firstly run for 5 ps with a time step of 1 fs. If no bond breakage or decomposition was observed, another 15 ps was added.

Figure 22a-c show the final structures of one molecule on the Li metal after the AIMD simulations. No reactions occur between DME and the Li metal after 20 ps (Figure 18a). In contrast, after 5 ps, one of the C-O bonds breaks in TMP (**Figure 22b**), forming a CH_3 radical, while the $LiNO_3$ completely decomposes to nitrides and oxides (**Figure 22c**). These observations are consistent with the SEM images for Li surfaces soaked in DME or TMP for 1 hour .

The DME/TMP/$LiNO_3$ interlayer synthesized by simple soak coating approach can form a soft organic-inorganic composite layer on Li metal surface. Such DTL interlayer can effectively protect Li metal by suppressing Li volume change during cycling. The interlayer can also uniformly distribute the stress generated during cycling. The reduced strain rate during the initial stage of plating can mitigate SEI delamination and cell failure. With the interlayer applied between Li and LLZO, intensive polishing is no longer necessarily needed. Further investigation is be focused on studying the chemical composition of the DTL layer and understanding the reaction mechanism and how the interlayer impacts the critical current density.

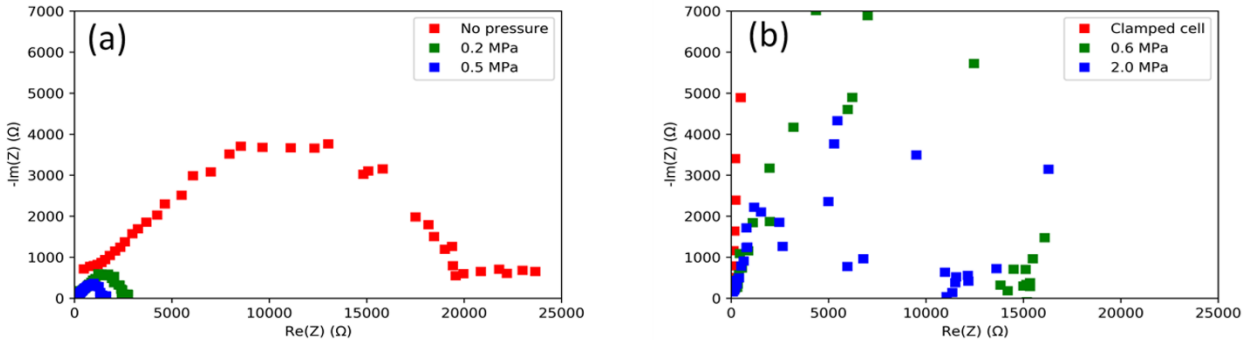

Figure 23 (a) EIS spectra taken on DTL-coated Li symmetric pouch cell. (b) Bare lithium symmetric pouch cell EIS data. The inset at the top right shows the spectra when the pouch cell is clamped. Note that the clamped cell interfacial impedance is too large to be shown on the plot in (b).

To help mitigate this surface layer formation and to decrease the interfacial resistance between lithium foil and the solid electrolyte in all-solid-state batteries, researchers are looking into coating an artificial solid-electrolyte interphase onto lithium foil. Here we present measurements on the interfacial resistance of coated lithium foil and its dependence on applied external pressure. Lithium foil was coated in a solution of Dimethyl ether, trimethylopropane, and Lithium Nitrate (DTL). DTL coated and uncoated lithium foil samples were prepared at GM. Samples were then assembled, and vacuum sealed in a pouch cell for pressure cell studies. **Figure 23** shows EIS data that suggests that the interfacial resistance significantly decreases when lithium foil is coated with DTL, and that under externally applied pressure both coated and uncoated samples show a significant decrease in their interfacial resistances.

4.6.2 Mechanical properties of interlayer materials

Determining the mechanical properties of interlayer materials is vital for long-term cycling in lithium metal batteries. It has been proposed that the shear modulus of a solid electrolyte in a solid-state lithium metal battery is an important parameter for preventing dendritic growth, for instance. The measured elastic modulus of nanoindentation experiments on thin films can be

influenced by the substrate. To see the influence of the substrate, environmental nanoindentation was performed on two different samples of dip-coated thin films grown on lithium foil using a Berkovich tip. **Figure 24** shows that the average modulus decreased as the dip-coat time increased, and that the modulus of the maximum dip-coat time sample of 2 hours is similar to the average results for the 1-hour sample. These results provide more confidence that the previous results found are probing the polymer film. **Figure 25** shows histograms representing the spread of the data comparing each sample with lithium foil.

The error bars in **Figure 24** show that the measured modulus varies significantly across every sample. For lithium foil, this may be explained by how Lithium has a very high anisotropy factor, and since lithium foil is polycrystalline, it is expected to see moduli ranging by 17 GPa. It is proposed that one reason for such large variations in the thin film samples has to do with variations in the morphology of the film. Figure 26 shows an example of three AFM images taken at different locations on the DME 15-minute sample, showing differences in the local morphology of the film at different locations.

It is also plausible that the sharpness of the Berkovich tip makes it difficult to detect the surface of such a soft polymer layer, as reported previously. To build more confidence in these results, flat punch indentation will be performed next. Creep studies will also be performed with this indenter to extract the time-dependent modulus to characterize the viscous behavior of the polymer film. These results will aim to better understand why coated lithium metal anodes outperform uncoated ones during long-term cycling tests. Finally, finite element method (FEM) will be applied to this system to determine whether the results presented here are in isolation of the substrate.

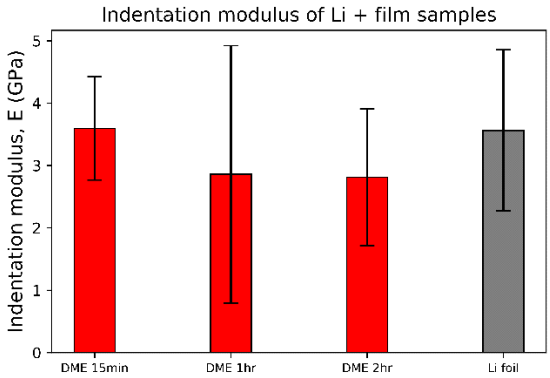

Figure 24. Indentation modulus results on different thin films on Li-foil.

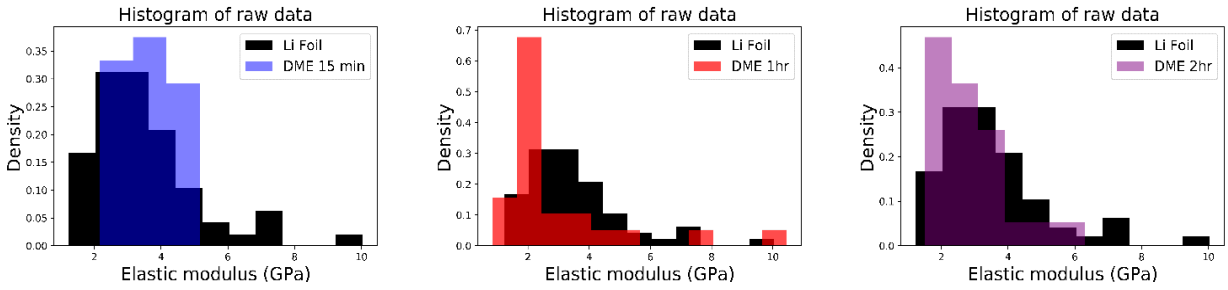

Figure 25. Histogram of the moduli in Figure XVI.14.8.

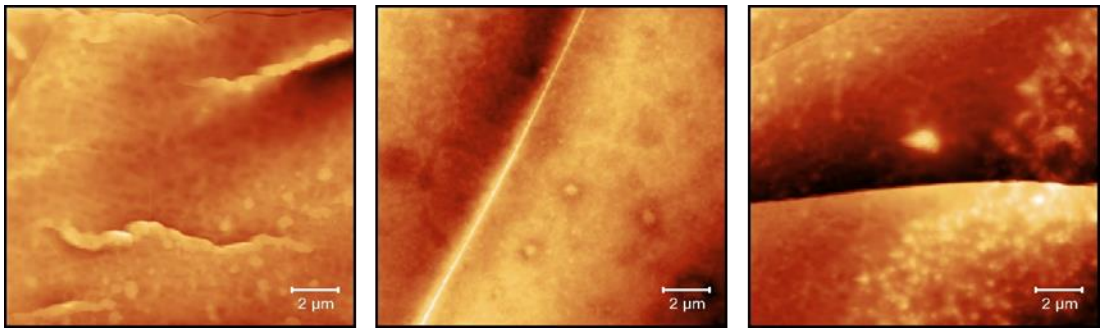

Figure 26. Three AFM images at different locations of the DME 2 hr. sample.

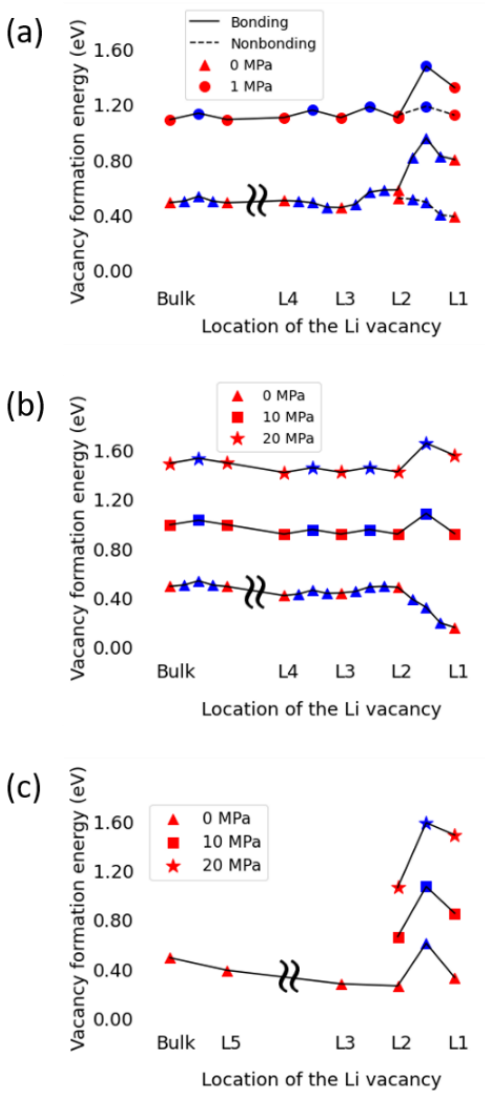

Figure 27. Forward and backward barriers for at different stack pressures for Li/Li_2O (a), Li/LiF (b) and Li/LLZO interfaces (c) for later KMC simulations. The red markers represent the vacancy formation energy and blue ones stand for the transition state energy. For the Li/LLZO interface, more NEB calculations will be performed to get all the necessary hopping barriers to perform the KMC simulations.

Figure 27 shows the forward and backward hopping barriers in the three Li/SE interfaces at different stack pressures. When the stack pressure is applied ($\sigma > 0\ MPa$), the forward hopping barrier (E_f) is decreased by half of the mechanical bias (E_p), while the backward hopping barrier is increased by half of E_p (the method to solve E_p from $\dot{n_p}$ will be summarized in the next quarter). For Li/Li_2O and Li/LiF interfaces, all the barriers have been calculated. For the Li/LLZO interface, more NEB calculations will be performed to get all the hopping barriers at 0 MPa and then the modified barriers can be obtained at different stack pressures.

With the modified barriers due to creep effects, the KMC simulations of the vacancy evolution during stripping can be performed at different stack pressures and provide the range of CCD. With the CCD and critical pressure predicted from the analytical model and the KMC simulations, the interface and creep effects on the Li surface morphology can both be studied and provide clues to design the Li/SE interface and keep it flat during stripping.

In addition, the optimized interlayers will be applied between Li metal electrode and solid electrolyte to test the critical current density. Based on that, the cycle life tests will be performed to investigate how the interlayer can improve the cycle stability of all solid-state batteries

5. SUMMARY OF PROJECT ACTIVITES

- Various techniques have been developed to study the dynamic phenomena at the interfaces of solid-state batteries. These include coating deposition techniques, in-situ techniques, and postmortem analysis capabilities. Successful deposition of LLZO thin films on different substrates has been achieved. Additionally, different configurations of electrode/SSE/electrode structures have been proposed to measure properties such as ionic conductivities.
- In-situ stress studies have directly shown that when Li metal penetrates LLZO, it leads to significant stress buildup in the solid electrolyte. Ongoing efforts aim to improve the quantitative interpretation of these studies, investigate materials with engineered residual stresses, and extend this approach to fully solid-state configurations.
- Multiscale models have been developed to understand the interaction between interfaces, diffusion, stripping current density, stack pressure, and contact area evolution during Li-stripping. These models have demonstrated that using a lithiophilic interlayer can reduce stack pressure and increase the critical current density required to prevent lithium dendrite growth.
- Pressure studies have shown that a soft and compliant artificial SEI (solid electrolyte interphase) layer, with a modulus much lower than LLZO, can further improve the initial interfacial impedance. These findings suggest that a softer viscoelastic interface between lithium and LLZO is better suited to improve the interfacial impedance.
- Interlayer design strategies have been established and verified through the coating of lithium anodes. Furthermore, different approaches have been explored to engineer the grain boundary, aiming to reduce sintering temperature and enhance ionic conductivity.

6. PRODUCTS DEVELOPED UNDER THE AWARD & TECHNOLOGY TRANSFER

6.1 PUBLICATIONS

1. J. Cho, K. Kim, S. Chakravarthy, X. Xiao, J. L. M. Rupp, B. W. Sheldon, An Investigation of Chemo-Mechanical Phenomena and Li Metal Penetration in All-Solid-State Lithium Metal Batteries Using In Situ Optical Curvature Measurements, Adv Energy Mater 12, 2200369 (2022)
2. T. Cai, A. S Westover, S. Kalnaus, J. Cho, C.E. Athanasiou, N. Dudney, and B. W. Sheldon, In-situ Thermo-Mechanical Characterization and Strain Engineering of Lipon Thin Films, to be submitted (June 2023).
3. A Meyer, X Xiao, M Chen, A Seo, YT Cheng, A Power-Law Decrease in Interfacial Resistance Between Li7La3Zr2O12 and Lithium Metal After Removing Stack Pressure, Journal of The Electrochemical Society 168 (10), 100522
4. A Seo, A Meyer, S Shrestha, M Wang, X Xiao, YT Cheng, Observation of the surface layer of lithium metal using in situ spectroscopy, Applied Physics Letters 120 (21), 211602
5. M. Feng, C. Yang, and Y. Qi, The Critical Stack Pressure to Alter Void Generation at Li/Solid-Electrolyte Interfaces during Stripping, Journal of The Electrochemical Society, 2022, 169, 090526
6. Y. Wang, D. Dang, X. Xiao, Y.-T. Cheng, Structure and mechanical properties of electroplated mossy lithium: Effects of current density and electrolyte, Energy Storage Materials, Vol. 26, 2020, Pages 276-282.
7. C. Yang, Y. Lin; B. Li, X. Xiao, Y. Qi, The Bonding Nature and Adhesion of Polyacrylic Acid (PAA) Coating on Li-metal for Li Dendrite Prevention, ACS Appl. Mater. Interfaces 2020, 12, 45, 51007–51015
8. Cho, J. H.; Xiao, X.; Guo, K.; Liu, Y.; Gao, H.; Sheldon, B. W., Stress evolution in lithium metal electrodes. Energy Storage Materials 2020, 24, 281-290.
9. C.T. Yang and Y. Qi, Maintaining a Flat Li Surface during the Li Stripping Process via Interface Design, Chemistry of Materials, 2021, 33, 2814–2823
10. M.W. Swift, J.W. Swift, Y. Qi, Modeling the electrical double layer at solid-state electrochemical interfaces, Nature Computational Science 2021, 1, 212–220

6.2 PATENT APPLICATIONS

1. Xingcheng Xiao, Robert Schmidt, Yifan Zhao, A simplified process to improve the ionic conductivity of solid electrolyte, U.S. Patent Application, 2023 (GM Ref. No. P104736)
2. Xingcheng Xiao, Yang-Tse Cheng, Thomas Yersak, Self-healing solid-state battery configuration and the method of manufacturing thereof. U.S. Patent Application No. 18/327464, 2023 (GM Ref. No. P104629)
3. Xingcheng Xiao, A process to reduce the interfacial impedance in all solid-state batteries, U.S. Patent Application No. 18/158719, 2023 (GM Ref. No. P103667)
4. Xingcheng Xiao, Mengyuan Chen, Qinglin Zhang, Mei Cai, A solution-based approach to protect lithium metal electrode, U.S. Patent Application No. 17/128974, 2020 (GM Ref. No. P053352)

5. Xingcheng Xiao, Mengyuan Chen, Methods for Forming Ionically Conductive Polymer Composite Polymer Interlayers in Solid-state Batteries, U.S. Patent Application No. 17/230788, 2021 (GM Ref. No. P054138)
6. Mengyuan Chen, Xingcheng Xiao, Composite Interlayers for Solid State Batteries and the Method of Making Same, U.S. Patent Application No. 17/307664, 2021 (GM Ref. No. P054203)

6.3 INVITED TALKS

1. Yue Qi, "Li electrochemical deposition and stripping kinetics and reversibility", 2023 Lithium Metal Workshop; Feb 2023, La Jolla, CA
2. Yue Qi, " The impact of Interface layer on Lithium Plating and Stripping Morphology", 241st ECS, May 2022, Meeting, Vancouver, BC, Canada
3. Yue Qi, " The impact of Interface layer on Lithium Plating and Stripping Morphology", SES Conference, Oct 2022, Texas A&M, TX
4. Yue Qi, "The Electrochemo-Mechanics of Interfaces in All-solid-state Li-ion Batteries", 2021 Virtual MRS Spring Meeting, April 2021
5. Brian W. Sheldon, “Interface Stability and Related Chemo-Mechanical Phenomena During Lithium Metal Plating”, Society of Engineering Science Annual Meeting, virtual, October 1, 2020.
6. Brian W. Sheldon, “Interface Stability and Related Chemo-Mechanical Phenomena During Lithium Metal Plating”, Oklahoma State University, Stillwater, Oklahoma, April 25, 2022.
7. Brian W. Sheldon, “Chemo-Mechanical Degradation of Energy Storage Materials”, CIRIMAT, Institut National Polytechnique de Toulouse, Toulouse, France, June 28, 2022.
8. Brian W. Sheldon, “Chemo-Mechanical Phenomena in Solid Electrolytes”, Multiscale Mechanics, Multiphysics Modeling and Simulations for Energy Storage (Euromech Colloquium 617), Sirmione, Lake of Garda, Italy, August 30, 2022.
9. Brian W. Sheldon, “Dendrite Mitigation and Chemomechanical Phenomena in Solid Electrolytes”, Society of Engineering Science Annual Meeting, Minneapolis, Minnesota, October,2023.
10. Brian W. Sheldon, “Chemomechanical Phenomena During Lithium Metal Plating”, 244th Electrochemical Society Meeting, Gothenburg, Sweden, October 2023. J-H Cho, X. Xiao, K. Guo, Y. Liu, H. Gao, and B.W. Sheldon, “In Situ Investigations of Stress Evolution During Plating and Stripping of Lithium Metal”, Fall MRS Meeting, virtual, November 2020.
11. J.-H. Cho, K. Kim, S. Chakravarthy, X. Xiao, J. Rupp & B.W. Sheldon, "In-situ Curvature Measurements Using LLZO Solid Electrolyte", 240th Electrochemical Society Meeting, Orlando, Florida, October 2021.
12. J-H. Cho, K. Kim, S. Chakravarthy, X. Xiao, J. Rupp, and B.W. Sheldon, “An Investigation of Chemo-Mechanical Phenomena in Solid Electrolytes Using In Situ Curvature Measurements”, Fall MRS Meeting, Boston, Mass, November 2021.
13. S. Morris, J.-H. Cho, K. Kim, X. Xiao, J.L.M. Rupp, and B.W. Sheldon, “Investigating Chemo-Mechanical Phenomena in All-Solid-State Lithium Metal Batteries using In Situ Curvature Measurements”, Fall MRS Meeting, Boston, Mass, November 2022 (Best Poster Award)

14. T. Cai, A. Westover, S. Kalnaus, N. Dudney, and B.W. Sheldon, “In-situ Thermo-Mechanical Characterization and Strain Engineering of LiPON Thin Films”, 243rd Electrochemical Society Meeting, Boston, Mass, May 2023.

7. ACKNOWLEDGMENT AND DISCLAIMER

This material is based upon work supported by the U.S. Department of Energy’s Office of Energy Efficiency and Renewable Energy (EERE) under the Vehicle Technologies Office Award Number DE-EE0008863.